J. Wind Eng. Ind. Aerodyn. 119 (2013) 102–113

Contents lists available at SciVerse ScienceDirect

Journal of Wind Engineering and Industrial Aerodynamics

journal homepage: www.elsevier.com/locate/jweia

Mean loads on vaulted canopy roofs

M.B. Natalini, C. Morel, B. Natalini *

Facultad de Ingeniería, Universidad Nacional del Nordeste, Av. Las Heras 727, 3500 Resistencia, Argentina

ARTICLE INFO

Article history:
Received 24 December 2012
Received in revised form
10 April 2013
Accepted 1 May 2013

Keywords:
Wind loads
Vaulted roofs
Canopy roofs
Wind tunnel
Mean pressures

ABSTRACT

The vaulted canopy roof (VCR) is a widespread structure used in vast areas of South America, especially in parts of Argentina, Brazil and Paraguay. Information about the aerodynamics of VCRs is scarce in the literature, and it is restricted to mean load coefficients, which must be used in combination with the quasi-steady approach. Most of the existing data have been produced during the last decade in South America, but these data are not readily accessible because they were published in Spanish. This paper presents the results of mean wind load coefficients on VCRs obtained in boundary layer tunnel tests, and the aerodynamics of VCRs are discussed by taking into account the data produced during the last decade.

1. Introduction

The vaulted canopy roof (VCR) is a widespread type of structure used in vast areas of South America, especially in parts of Argentina, Brazil and Paraguay, where the climate is warm. VCRs are used as shelters in schools, sport facilities, carpenter's workshops and car parks in both urban and rural areas.

VCRs are not considered by any wind loads code of practice currently in use. However, in the past, two codes provided recommendations for VCRs: the French code NV 65 (1970) and the Argentinean code CIRSOC 102 (1983), the former having been superseded by the Eurocode and the latter being superseded by a newer version (CIRSOC 102, 2005). Both codes suggested using the same mean pressure coefficients for planar canopy roofs having the same rise/span relationship, a suggestion with no basis in the literature. Indeed, Marighetti et al. (2002) showed that this approximation is incorrect in their presentation of wind tunnel results of the mean pressure distributions on VCRs, which they compared with those corresponding to a duo-pitch planar canopy roof with similar aspect dimensions.

The aerodynamics of VCRs remain largely unknown due to a lack of available data. Cook (1990) formulated the only conceptual framework currently in existence to characterise the wind loads over VCRs, exploiting the information available at that time as much as possible; unfortunately, however, this information was very scarce. Cook (1990) summarised the situation when he wrote, 'There are only small amounts of data for curved canopies and these are all early data obtained in smooth uniform flow. For example Irminger and Nokkentved included a barrel vault canopy with a rise of $r=W/4$ in their studies published in 1936, and Blessmann included domed canopies with rises W/4 and W/8 in his 1971 studies. The validity of the loading coefficient is open to question in the light of current techniques, however the general loading characteristics may be still be useful.' Twenty years after the publication of Cook's commentary, the situation is virtually unchanged. Conversely, the planar canopy roof (PCR) is a morphology that has been studied in several institutions during the last thirty years. Although the number of studies is relatively small in absolute terms, currently, the aerodynamics of PCRs are well-established in terms of state-of-the-art wind engineering. Altogether, the full-scale tests of Dryton and Silsoe in the early 80s (Robertson, Hoxey and Moran, 1985), Oxford (Gumley and Wood, 1980; Gumley, 1981, 1982,1984; Belcher and Wood, 1983), Queensland (Ginger and Letchford, 1991), Clemson (Altman, 2001), Concordia and Tohoku (Uematsu et al., 2007) cover a wide range of geometries, blockage effects and measurement techniques. The results of these studies are incorporated into several codes, including, among others, the Eurocode, the ASCE 7, the Australian/New Zealand, the Canadian and the Argentinean codes.

Currently, apart from the early data of Irminger and Nokkentved (1936), the only reports of wind tunnel tests on VCRs are from the Universidad Nacional del Nordeste (UNNE), Argentina. These tests were conducted in the 'Jacek P. Gorecki' boundary layer wind tunnel using wind simulation. The sensitivity of the VCR models to the Reynolds number, the roughness of the roof and the incoming turbulence was studied by Natalini et al. (2001), who tested three models of VCRs and two models of enclosed buildings using different wind simulations. They showed that suitable

* Corresponding author. Tel.: +543624439039; fax: +543624428106.
E-mail address: bnatalini_2000@yahoo.com.ar (B. Natalini).

0167-6105/$ - see front matter © 2013 Elsevier Ltd. All rights reserved.
http://dx.doi.org/10.1016/j.jweia.2013.05.001

modelling conditions can be obtained in the UNNE tunnel by adding sand on the upper side of the models to force the transcritical regime and by using a suburban wind simulation. Marighetti et al. (2002) compared the pressure coefficients on the top surface of models of a VCR and a PCR and confirmed that they are different, as previously stated by Cook (1990). Natalini et al. (2002) tested models of a VCR and an enclosed building with a curved roof to show the difference of the pressure distributions. Natalini et al. (2005) presented test results from three different VCR models and proved that the most severe net mean loads appear under wind directions of 90°, 75° and 60° relative to the ridgeline. Balbastro and Sonzogni (2006, 2007) tested four VCR models using a novel technique to build the models, which eliminated any possible interference between the pressure tubing connections and the flow. They also presented results of numerical models of similar dimensions, which were compared to the experimental results. Regarding computational modelling, there are two previous works by Balbastro et al. (2004, 2005) in which some of the UNNE experiments were reproduced using a Large Eddy Simulation (LES) model with some success. In 2006, the numerical model was fully calibrated, and results were produced using a variety of aspect ratios, which were reported by Balbastro and Sonzogni (2006, 2007, 2011, 2012) and Balbastro (2009). Further details of these studies are shown in Table 1 and Section 6. All the data provided by these studies are limited to time-averaged coefficients, necessitating the use of the quasi-steady theory.

Table 1
Summary of previous studies.

Authors	Subject of the study	Testing methodology	Aspect relations of the models			Terrain/wind angles (0° refers to the along-the-ridge direction)	Scale	Type and format of data presented
			f/b	h/b	a/b			
Irminger and Nokkentved (1936)	Net loads on a VCR.	Wind tunnel test.	0.25	N/A	N/A	Smooth and uniform flow/ 90°–60°–30°	N/A	Area-averaged net pressures on six strips of roof along the axis of the barrel.
Natalini et al. (2001)	The sensitivity of VCRs models to the Reynolds number, the roughness of the roof and the incoming turbulence.	Wind tunnel tests with and without wind simulation at 7 different Re. Two models with sand on the roof and one with smooth roof.	0.17	0.5	2.2	Suburban area/90°	1:75	Upside point pressures: distributions across middle section. Drag force: variation with Re.
Marighetti et al. (2002)	Comparison of upside pressures on a VCR and a PCR of similar dimensions.	Wind tunnel tests. Wind simulation. Models with sand on the roof.	0.17	0.5	2.2	Suburban area/90°-45°	1:75	Upside point pressures: contour plots.
Natalini et al. (2002)	Net loads on a VCR and comparison with enclosed building of similar dimensions.	Wind tunnel tests. Wind simulation. Models with sand on the roof.	0.17	0.5	2.1	Suburban area/ 90°-45°	1:75	Upside, downside and net point pressures: contour plots and distributions across three different sections.
Balbastro et al. (2004, 2005)	Calibration of CFD tool.	CFD-3D modelling. Finite Element Model (FEM) and Large Eddy Simulation (LES).	Reproduction of experiments reported by Natalini et al. (2001, 2002)					Upside, downside and net point pressures: contour plots, distributions across different sections and flow visualisations.
Natalini et al. (2005)	To establish the most adverse wind directions	Wind tunnel tests. Wind simulation. Models with sand on the roof.	0.2	0.4 0.3 0.1	4	Suburban area/90°-75°-60°-30°-45°	1:75	Net point pressures: contour plots. Lift and drag force coefficients.
Natalini (2005)	Parametric study of the loads.	Wind tunnel tests. Wind simulation. Models with sand on the roof.	0.2	0.4 0.3 0.1	4 2	Suburban area/90°–75°–60°–30°–45°–30°–15°–0°	1:75	Net point pressures: contour plots and distributions across different sections. Lift and drag force coefficients.
Balbastro and Sonzogni (2006)	Test of novel tubing system. Calibration of CFD tool.	Wind tunnel tests. Wind simulation. Models with sand on the roof. CFD-3D modelling.	0.18	0.5	2.4	Suburban area/90°	1:75	Upside, downside and net point pressures: contour plots.
Balbastro and Sonzogni (2007)	Test of novel tubing system. Calibration of CFD tool.	Wind tunnel tests. Wind simulation. Models with sand on the roof. CFD-3D modelling.	0.18	0.5	2.4 1.2	Suburban area/90°	1:75	Upside, downside and net area-averaged pressures on six zones.
Balbastro (2009).	Parametric study of the loads.	CFD-3D modelling.	0.07 0.07 0.07 0.13 0.13 0.13 0.18 0.18 0.18	0.46 0.18 0.11 0.82 0.33 0.20 1.18 0.47 0.29	0.5 3.0 5.5 3.0 5.5 0.5 5.5 0.5 3.0	Suburban area/ 90°–60°–75°	1:75 1:1	Upside, downside and net area-averaged pressures on six zones. Flow visualisations.
Balbastro and Sonzogni (2011)	Influence of partial blockage.	CFD-3D modelling. One blockage arrangement.	0.12	0.5	2	Open country/90°	1:50	Lift and drag coefficients. Flow visualisations.
Balbastro and Sonzogni (2012)	Influence of partial blockage.	CFD-3D modelling. Twelve blockage arrangements (see Table 5).	0.12	0.5	2	Open country/90°	1:50	Lift and drag coefficients. Flow visualisations.

Admittedly, this theory is far from being the best load assessment model, but as long as no peak pressure data are available, quasi-steady theory is currently the only possible option. However, the purpose of this paper is not to provide design coefficients, but to improve our knowledge of the VCR aerodynamics by taking Cook's framework as a starting point.

In this work, new values of time-averaged load coefficients for VCRs obtained in wind tunnel tests are presented, and the aerodynamics of VCRs are discussed, taking into account the data produced during the last decade and the limitations imposed by the quasi-steady theory.

2. Experimental arrangement

Six 1:75 scale models were constructed in which geometry and size are in accordance with the range of VCR dimensions found more frequently in northeastern Argentina. Fig. 1 and Table 2 summarise the models' geometry. To calculate the Reynolds number (shown in Table 2), it was necessary to adopt a characteristic length, L, which was adopted to be $L=2r$.

The rise, f, and the span, b, were kept similar in all models. Basically, two types of models were built, long ones (A, B and C) and short ones (D, E and F), which allowed for the assessment of the influence of the length, a. By varying the heights of the eaves, h, (2, 4 and 6 cm), the six models were produced. Models C and F, with an h dimension that corresponds to 1.5 m at full-scale, do not represent any real situation. They have been included in the tests in order to observe the trends that the pressures follow when varying the height of the eaves.

The roof of the models was made from a 2-mm-thick aluminium plate, and the columns used 2.5-mm-diameter steel rods (except one column, the farthest one from the area where taps were placed, which had a square cross section of 10×10 mm). Because the models had two axes of symmetry, only a quarter of the roof had pressure taps in place, thus reducing the number of tubes needed. In addition, all the tubes were led towards the farthest column, through which they reached the floor, thus minimising the scale distortion in both the columns and the roof thickness and the possible interference of the tubes on the measurements. Figs. 2 and 3 summarise the positions of the pressure taps on the roof of the models.

To obtain flow in transcritical conditions, sand was added to the upper side of the roof of the models, which had a relative roughness, k/d, equal to 3.30×10^3. The choice of sand was based on the mean pressure data of models with different roughnesses, which were discussed by Natalini et al. (2001). This subject deserves further measurements of fluctuating pressures as well as full-scale data to validate the suitability of the modelling conditions. Both issues will be addressed at the UNNE, but presently, and as long as no further information is available, the best option, in the authors' opinion, is the one used in the present tests.

Fig. 4 The experiments were conducted in the 'Jacek P. Gorecki' wind tunnel at the Universidad Nacional del Nordeste. This is an open return wind tunnel with a working section of 22.4 m in length $\times$ 2.4 m in width $\times$ 1.8 m in height and a maximum flow velocity of 25 m/s when the working section is empty. A more detailed description of the tunnel is available in Wittwer and Möller (2000).

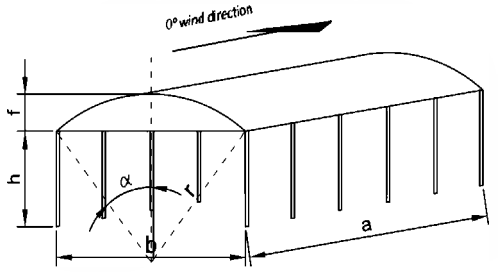

Fig. 1. Model geometry.

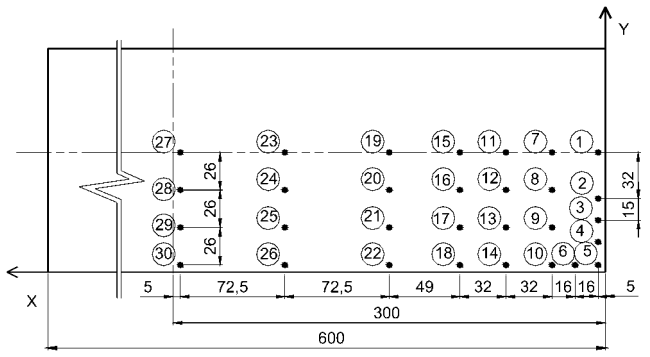

Fig. 2. Pressure taps distribution on models A, B and C. Dimensions are in mm.

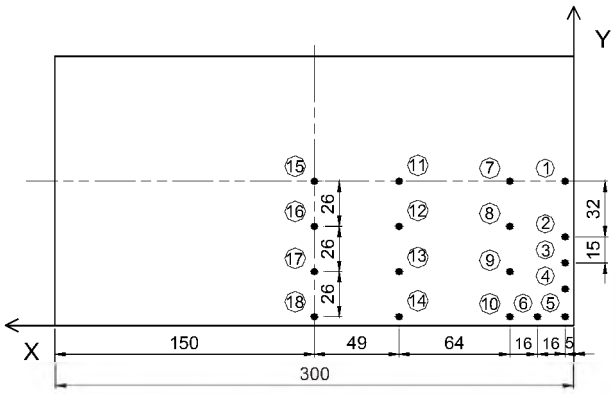

Fig. 3. Pressure taps distribution on models D, E and F. Dimensions are in mm.

Table 2
Model dimensions.

Model	Dimensions				Ratios				r (cm)	α	Re $\times 10^5$
	a (cm)	b (cm)	h (cm)	f (cm)	b/a	h/b	f/b	f/h			
A	60	15	6	3	0.25	0.40	0.20	0.50	10.88	43°58'	2.09
B	60	15	4	3	0.25	0.27	0.20	0.75	10.88	43°58'	1.96
C	60	15	2	3	0.25	0.133	0.20	1.50	10.88	43°58'	1.68
D	30	15	6	3	0.50	0.40	0.20	0.50	10.88	43°58'	2.09
E	30	15	4	3	0.50	0.27	0.20	0.75	10.88	43°58'	1.96
F	30	15	2	3	0.50	0.133	0.20	1.50	10.88	43°58'	1.68

Fig. 4. View of model A on the turntable.

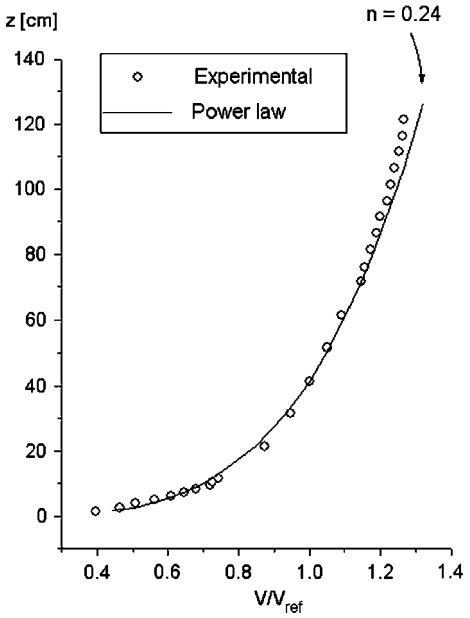

Fig. 5. Mean velocity profile.

All the models were tested under wind simulation conditions corresponding to a suburban area. The simulation hardware consisted of two modified Irwin's spires (Irwin, 1981) and 17.1 m of surface roughness fetch downstream from the spires, obtaining a part-depth boundary layer simulation of neutrally stable atmosphere. Each spire consisted of a trapezoidal frontal plate reinforced with a transversal plate on its leeward face, which is similar to an Irwin spire but with the upper part truncated. The size of the spires was determined by trial and error. The surface roughness was composed of wooden block elements 30 mm × 30 mm × 22 mm high mounted at a packing density of 15%. Fig. 5 shows the mean velocity profile of the simulation and a power law profile of exponent $n=0.24$. Fig. 6 shows the local turbulence intensities of the simulation together with atmospheric data after Helliwell (1971), Teunissen (1977), Lumley and Panofsky, Singer, Shiotani and Davenport and Isyumov (Counihan, 1975), which correspond to suburban areas. Fig. 7 presents the power spectrum measured at an elevation of 38.4 cm, and Figs. 8 and 9 show the values of the integral scale and the model scale factor of the wind simulation, respectively, of the longitudinal component of the turbulence. The model scale factor was obtained through Cook's procedure (Cook, 1977/1978). De Bortoli et al. (2002) provided further details for this simulation, including design criteria, size, geometry and arrangement of the hardware.

Point pressures were measured using a differential pressure electronic transducer (Micro Switch Honeywell 163 PC). Measurements on the upper and lower sides were not simultaneous. The pressure taps were alternatively connected to the transducer via a sequential switch Scanivalve 48 D9-1/2 with PVC tubes of 1.5 mm internal diameter and 400 mm length. No resonance problems

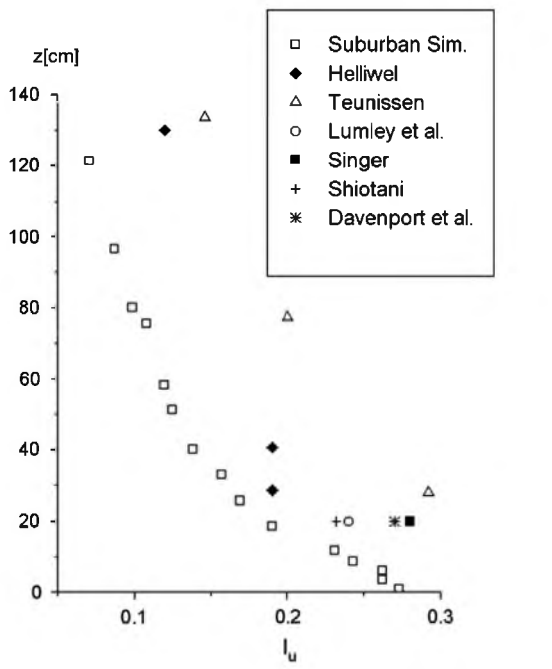

Fig. 6. Local turbulence intensities.

were detected in tubes of that specific length (gain factor≅1); therefore, restrictors of section were not used for filtering. The DC transducer output was read with a Keithley 2000 digital multimeter. The integration time operation rate of the analog-to-digital converter was set to obtain mean values over 55 s of real time integration.

Simultaneous to the pressure measurements being taken on the roof, the reference dynamic pressure, q_{ref}, was measured at the height of the eaves with a Pitot-static tube connected to a Van Essen 2500 Betz differential micromanometer with 1 Pa resolution. The probe was located beside the model at a distance of approximately 70 cm to avoid mutual interference. The reference static pressure was obtained from the static pressure tap of the same Pitot-static tube.

3. Results

Time-averaged pressure coefficients were measured under incoming wind at 60°, 75° and 90° angles relative to the ridgeline because these directions produce the most severe mean loads, as demonstrated by Natalini et al. (2005).

The net pressure coefficient, c_p, was obtained by subtracting the pressure coefficient on the lower side (downside), $c_{p\mathrm{D}}$, from the pressure coefficient on the upper side (upside), $c_{p\mathrm{U}}$. These last two coefficients are the rates between the pressure on the tap, p, which can be either an upside or downside pressure, and q_{ref}, which is the reference dynamic pressure measured at the reference height. Here, the tap pressures are relative to the static reference pressure, p_{ref}, which is obtained from the static tap of the same Pitot-static tube used to measure q_{ref}. Following the usual convention, negative values of $c_{p\mathrm{U}}$ indicate actions directed away from the upper surface (suction), while negative values of $c_{p\mathrm{D}}$indicate actions directed away from the downside surface. Accordingly, positive values of c_p indicate actions directed downwards.

The whole set of results of the experiments were provided by Natalini (2005). The short models (A, B and C) produced values on the same order of magnitude with similar patterns. The same correlation between results was observed for the long models (D, E and F). Conversely, some differences have been observed, though

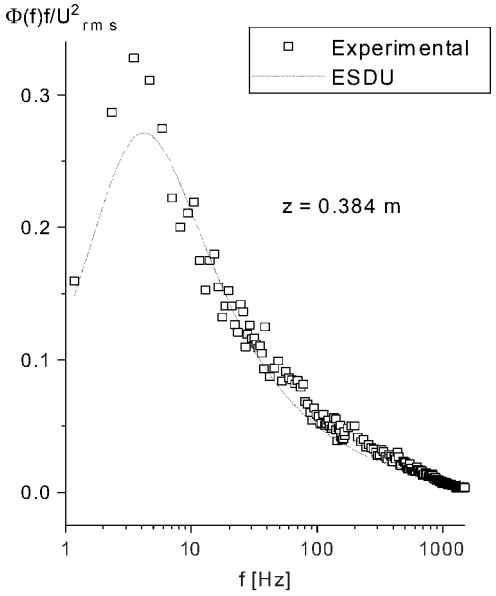

Fig. 7. Typical power spectrum. The dotted line is the atmospheric spectrum from ESDU.

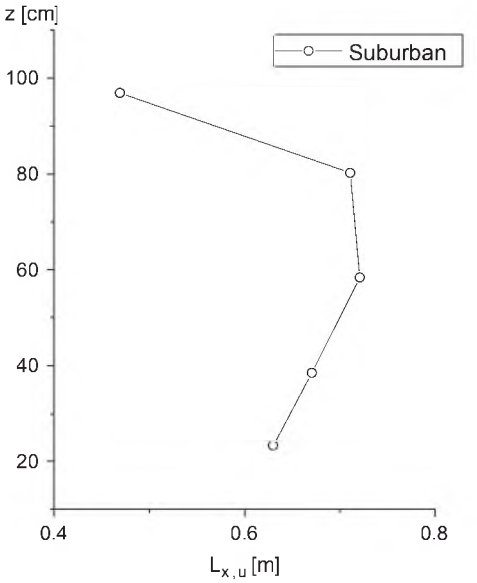

Fig. 8. Integral scale.

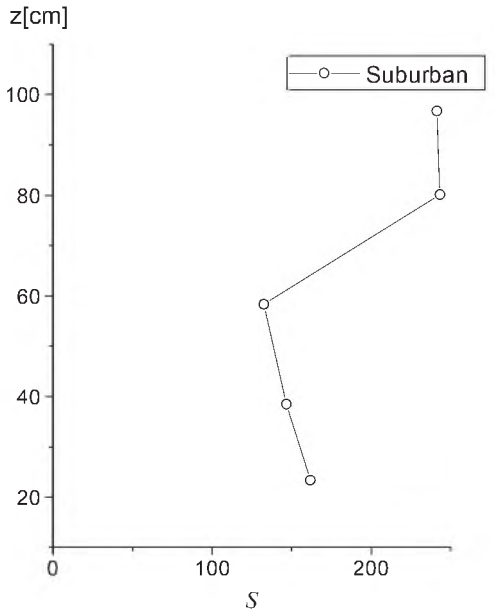

Fig. 9. Scale factors.

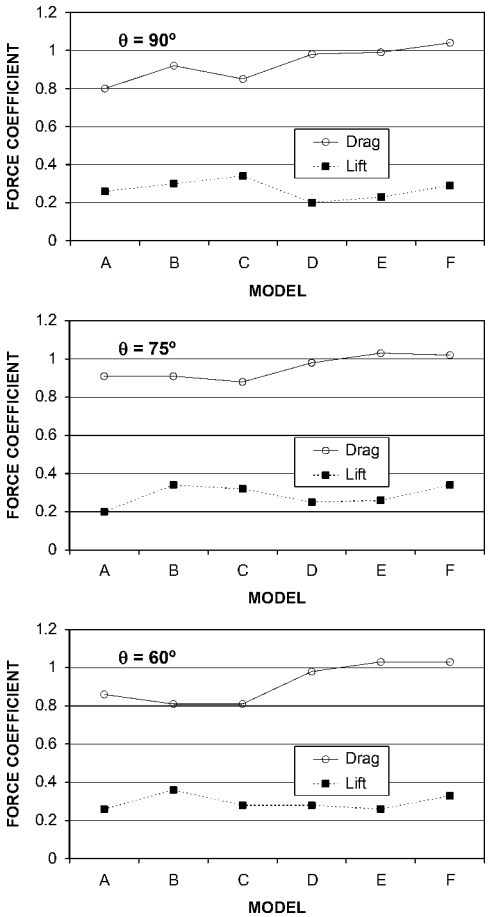

Fig. 10. Drag and lift coefficients, C_D and C_L, on the whole roof.

not dramatic, between short and long models. Fig. 10 shows the drag and lift coefficients, C_D and C_L, on the whole roof, which were obtained by integrating the pressure coefficients over the roof. Regardless of the wind direction, the values of C_L ranged from 0.2 to 0.4, and C_D ranged from 0.8 to 1.05. No major influence of the aspect relation h/b (eave height/span) is observed on the global coefficients. The maximum variations with h/b are on the order of magnitude of 0.1, and no clear trend in variations can be observed. Regarding the influence of the b/a ratio (span/length), the order of magnitude of the maximum variations between the long and short models is 0.1 for C_L and 0.2 for C_D. There is a trend toward more drag over short models.

Both aspect ratios, eave height/span and roof length/span, play fundamental roles in the load coefficients over vaulted roofs of enclosed buildings (Blessmann, 1998; Blackmore and Tsokri, 2006). Therefore, it is worthwhile to look at the causes of the observed differences in lift and drag before going into the details of the pressure coefficient distributions. Let us consider, for instance, models A and D under a wind direction of 90° (normal to the ridge). Consider that both models have the same dimensions, but model A is twice as long as model D. C_L and C_D in these two cases differ by 0.1 and 0.2, respectively. Fig. 11 compares the

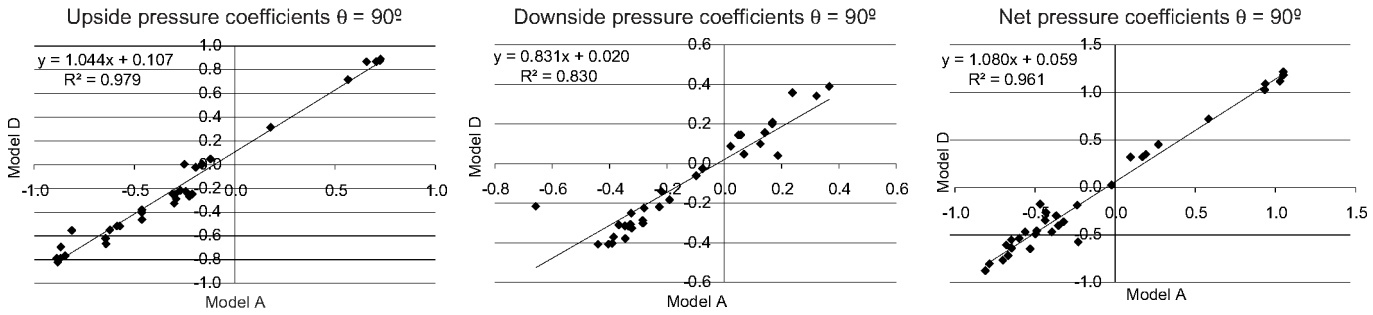

Fig. 11. Comparison of pressure coefficients on models A and D under incident wind at 90°.

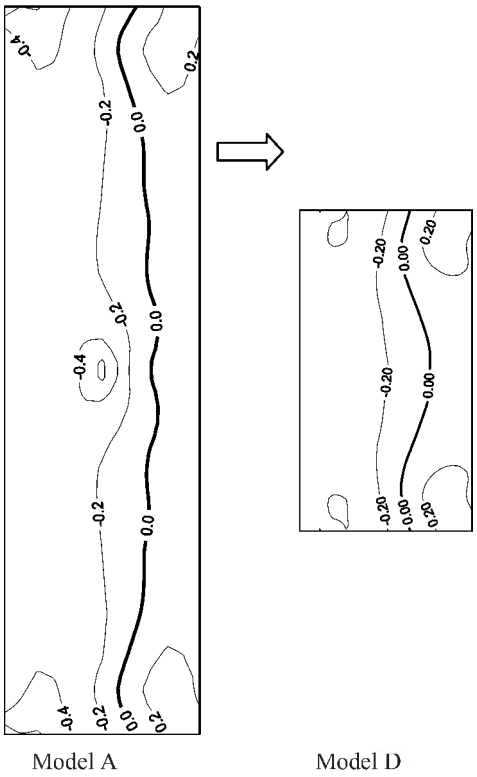

Fig. 12. Downside pressure coefficient contour plots—wind direction 90°.

values of c_{pU}, c_{pD} and c_p measured at equivalent points. A straight line of best fit, obtained by linear regression, has been added. The comparison of the upside pressure coefficients among the models shows better agreement than the downside ones, though the best fit line of the upside pressures is shifted to the left, which means that the absolute values of c_{pU} in model D are greater than in model A, by a value of approximately 0.1. Actually, the correlation between values of c_{pU}, which is quantified by the square of the Pearson product-moment correlation coefficient (R^2 in the figure), is as high as 0.979, while it is 0.83 for c_{pD}.

Fig. 11 more clearly shows the differences among pressures on the models than the contour plots of the pressure coefficients, which are displayed in Figs. 12 and 13.

The differences between the downside pressures, which are easily appreciated in Fig. 11, are not as obvious in the contour plots, which look very similar. As expected, the upper pressure coefficients are virtually identical.

If the same analysis is conducted for the same models but under wind at 60°, as seen in Fig. 14, the difference of 0.12 observed among the values of C_D is explained by changes in the downside pressure distributions. In this case, the difference between the c_{pD} contour plots (Fig. 15 and 16) is evident: the underneath flow observed in approximately the middle third of model A does not have enough room to develop in model D.

Similar comparisons have been conducted on other pairs of models with the same results: the upside pressures are relatively similar, while the downside pressures are slightly less correlated.

Profiles of the pressure coefficient distributions on two different cross-sections of the long model A and the short model D are displayed in Figs. 17–22. Section I is a cross section located 5 mm inwards from the upwind edge (for the oblique wind direction), while Section II is in the middle of the roof. In every figure, profiles corresponding to the upside, downside and net pressure coefficients are superimposed.

It can be seen that the only noticeable difference between the two models is that there is a lobe of negative downside pressures on the ridge of the A (long) model, but only in Section II. As the upside pressure coefficients are similar in both models, the resulting net pressure coefficient profile is less negative in the long model.

Note that the contributions of the downside pressures range from 29% to 69% of the net pressures. The results presented here correspond to models with no blockage. Downside pressures are highly dependent on blockage conditions; therefore, loads can be expected to be significantly different under any degree of blockage. The way in which this can occur is discussed in the next section.

4. Revisiting cook's framework

According to the authors' knowledge, Cook (1990) proposed the only existing framework that fully describes the aerodynamics of VCRs. By carefully analysing the small amount of data available on a barrel-vault canopy tested in smooth uniform flow by Irminger and Nokkentved (1936), in addition to the mass of information produced in Great Britain by the National Institute of Agricultural Engineering (NIAE) and the Oxford University on PCRs in the early eighties (Robertson, Hoxey and Moran, 1985; Gumley and Wood, 1980; Gumley, 1981, 1982,1984; Belcher and Wood, 1983), he managed to produce a picture of the general characteristics of the mean loads on VCRs. In this section, the statements of Cook are discussed in light of the data presented in this paper and those from the following sources: Natalini et al. (2001, 2002), Natalini (2005), Balbastro (2009) and Balbastro and Sonzogni (2006, 2007, 2011, 2012).

4.1. General pattern of load

'In all cases there is a small lobe of positive (inward) load near the front of the canopy, but the majority of the canopy has a negative (outward) normal load.'

The results presented in the previous section and the data from all the other sources consistently confirm this assertion, though the interpretation of the term 'small lobe' can be deceiving. It would be more appropriate to say that in all cases, there is a fringe in the front of the canopy, comprising approximately one-fourth of the surface of the roof, where the load is positive.

4.2. Flow separation

'At $\theta=90^\circ$, the distribution shows the characteristic peak suction near the crest followed by a drop to a constant value, indicating flow separation similar to that for a circular cylinder…In the other skew wind directions, for which the effective rise/width ratio is reduced, there is no flow separation. This indicates that the rise/width ratio of f/b=0.25 is near the critical for separation, with higher rises giving separation and a loading distribution similar to a circular cylinder, and lower rises maintaining attached flow and behaving like a cambered wing.'

In general terms, this statement is valid, but Fig. 22 shows that for f/b=0.2, the flow still separates, as in the case of the circular cylinder. Visualisations of the flow past the cross-sections of canopies of f/b=0.126 and f/b=0.07 produced by Balbastro (2009) show that the flow still separates for f/b=0.126 but not for f/b =0.07, which indicates that the critical value of f/b for separation is not 0.25 but is approximately 0.1.

4.3. Local high loads

'For the barrel-vault, the local regions of the equivalent duopitch canopy can be used, with the exception of the ridge region 'F' which does not exist because there is no abrupt change of slope and the load distribution is continuous over the arc.'

All the sources confirm that the load distribution is continuous over the arc of VCRs. As for the values of the coefficients, Table 3 compares the most severe net pressures on model D and one duo-pitch PCR model tested by Ginger and Letchford (1991). Both models had similar size and aspect ratios. The PCR had a slope of 22.5° and aspect ratios f/b=0.21, h/b=0.36 and a/b=1.1 and was tested under

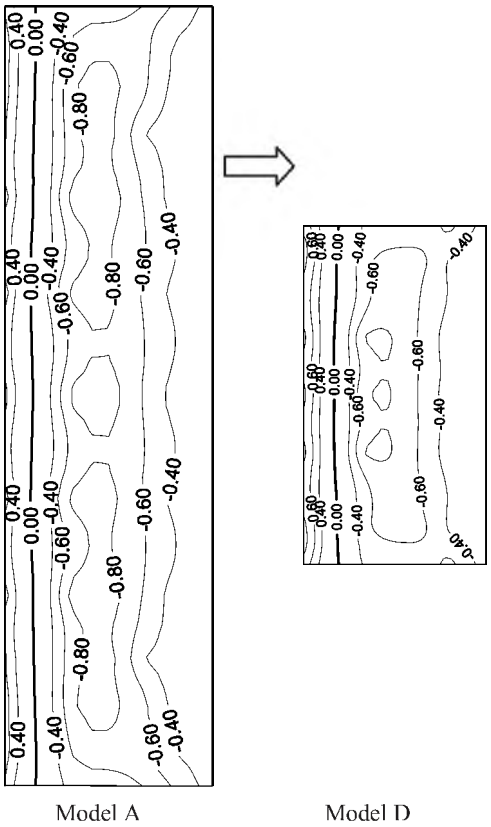

Fig. 13. Upside pressure coefficient contour plots—wind direction 90°.

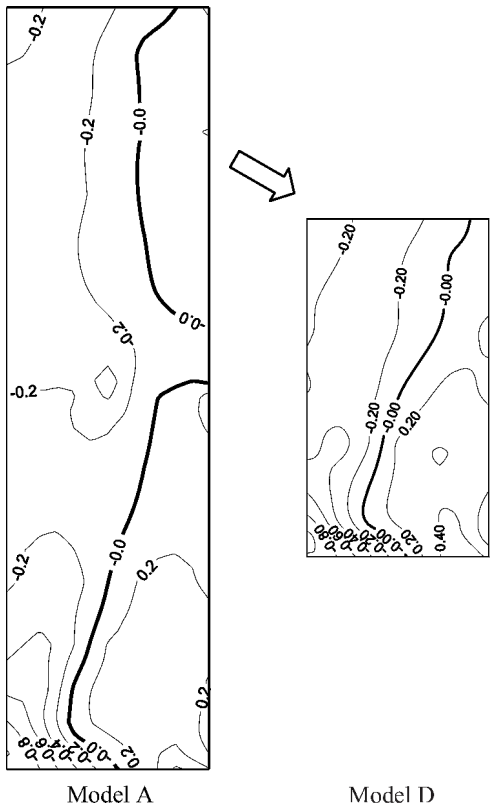

Fig. 15. Downside pressure coefficient contour plots—wind direction 60°.

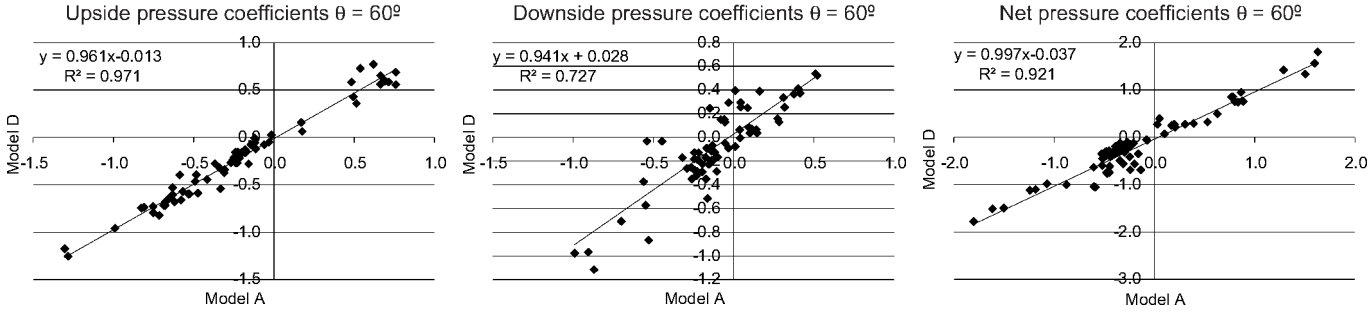

Fig. 14. Comparison of pressure coefficients on models A and D under incident wind at 60°.

a suburban wind simulation. The results presented in Table 3 are point mean pressures, with no blockage in any case. The densities and distributions of pressure taps were similar (though not identical) in both cases. The PCR model was tested under 0°, 30°, 60° and 90° wind directions. The most severe pressures occurred at 60°, similar to the VCR case. Table 3 confirms that near the ridge, the highest suctions are less severe on the VCR (half the value of the one on the PCR). Near the edges, some differences are observed, though not as marked as those closer to the ridge. In both models, the highest positive and negative pressures occurred at similar points (on one of the upwind edges). These pressures differ in absolute value by 0.4, but the suctions are more severe on the PCR, while the positive pressures are more severe on the VCR. The same trends were observed by Marighetti et al. (2002) concerning the upside pressures. They tested a 1:75 scale model of the Silsoe Dutch barn, which was a full-scale duo-pitch PCR (Robertson, Hoxey and Moran, 1985) studied in Great Britain. After ensuring that the full-scale mean loads were properly reproduced, they tested a VCR of identical aspect ratios using similar experimental conditions. Fig. 23 reproduces two figures from their work where the upside pressures for a wind direction of 45° are compared.

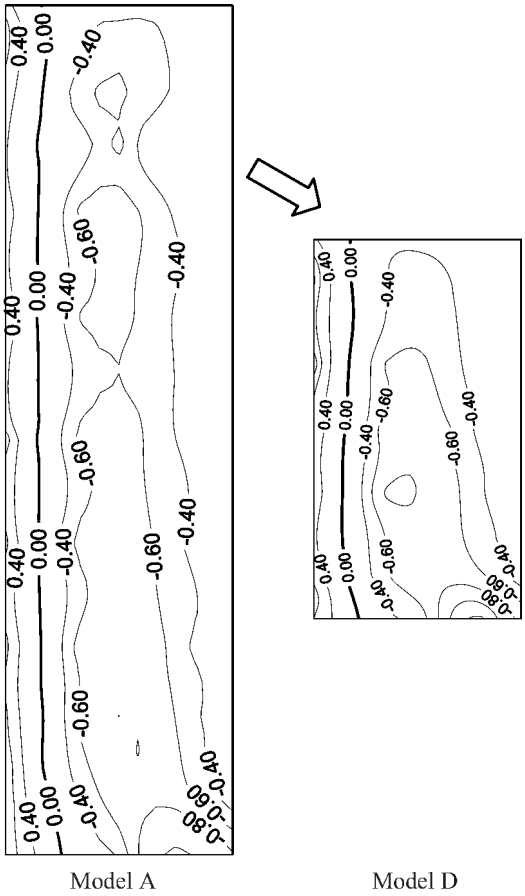

Fig. 16. Upside pressure coefficient contour plots—wind direction 60°.

4.4. Under-canopy blockage

Cook derived a set of rules for considering the effect of blockage from the data of the NIAE and Oxford experiments. Strictly speaking, the rules apply to PCRs. Because the blockage has a decisive influence on the resulting net load, it is discussed here whether these rules may be valid for VCRs.

4.4.1. Full blockage

The first rule concerns fully blocked canopies, that is, when the solidity ratio, *s*, which is the ratio of the total projected area or 'shadow area' of the stored goods to the projected area of the outside shape or 'envelope' of the structure, is equal to 1: '*... the loading of a fully blocked canopy may be determined in the same manner as an open-sided building, which is by taking the external pressures for the equivalent monopitch or duopitch building in combination with a suitable internal pressure.*' The suitable downside pressure recommended by Cook is shown in Table 4.

For duo-pitch PCRs, the validity of this rule is based in the following facts:

a) When there is no blockage, the upside pressure on the front upwind quarter of the roof is positive (downward), and it reverses to negative along the rest of the roof.
b) Under a full-blockage condition, the upside pressure distribution is identical to that of enclosed duo-pitch buildings.
c) Under any arrangement of full blockage, the upside pressure on the front upwind quarter of the roof changes from positive to strongly negative, but the pressure on the rest of the roof remains unchanged.
d) Under any arrangement of full blockage, the downside pressure becomes uniform, and its value will vary according to Table 4.

If similar trends would occur for VCRs, it could be expected that the rule for full blockage is also applicable. All the available sources confirm that condition (a) is similar in VCRs. Unfortunately, it is not possible to either confirm or reject conditions (b) and (c) when they are considered separately due to lack of data because, to date, no one has reported any results on the pressure distribution of any case of fully blocked VCRs. However, there is evidence that the conditions cannot be completely fulfilled by VCRs if they are considered altogether. The upside pressure distribution on VCRs on the two-thirds down-wind area, where the pressure is negative, is not identical to the external pressures

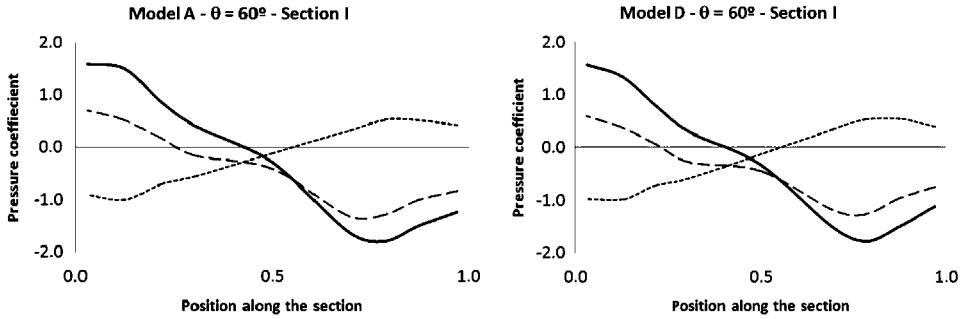

Fig. 17. Upside (dashed line), downside (dotted line) and net (solid line) pressure coefficient profiles. θ=60°. Upwind edge.

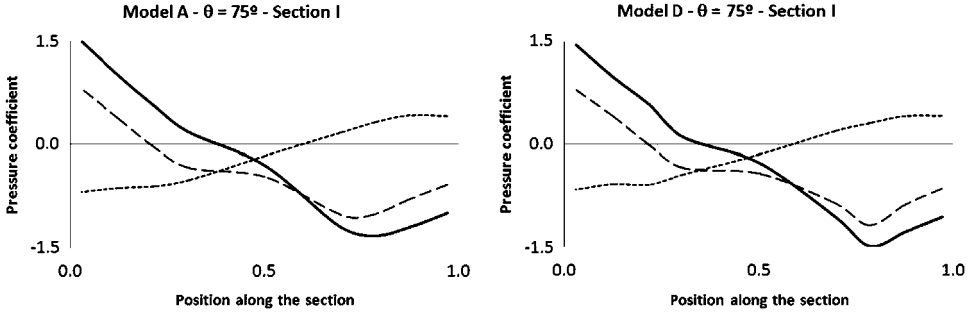

Fig. 18. Upside (dashed line), downside (dotted line) and net (solid line) pressure coefficient profiles. $\theta=75°$. Upwind edge.

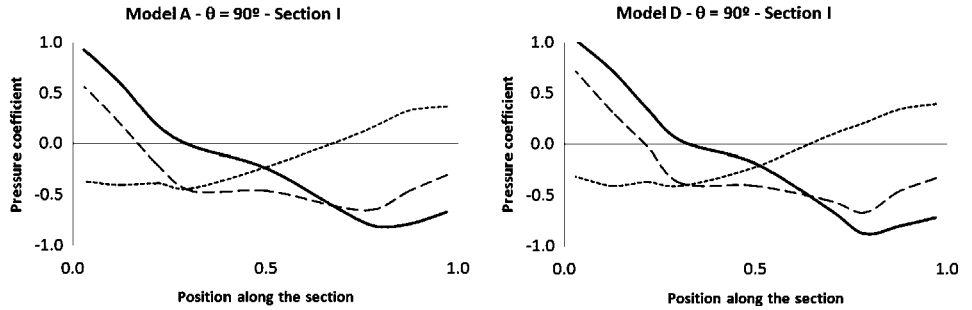

Fig. 19. Upside (dashed line), downside (dotted line) and net (solid line) pressure coefficient profiles. $\theta=90°$. Upwind edge.

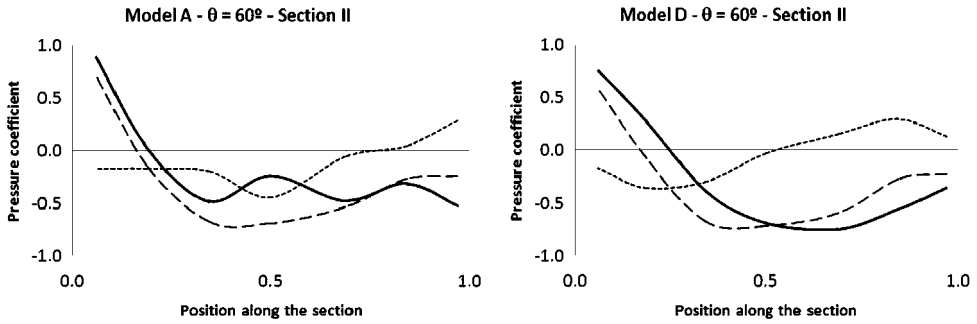

Fig. 20. Upside (dashed line), downside (dotted line) and net (solid line) pressure coefficient profiles. $\theta=60°$. Central section.

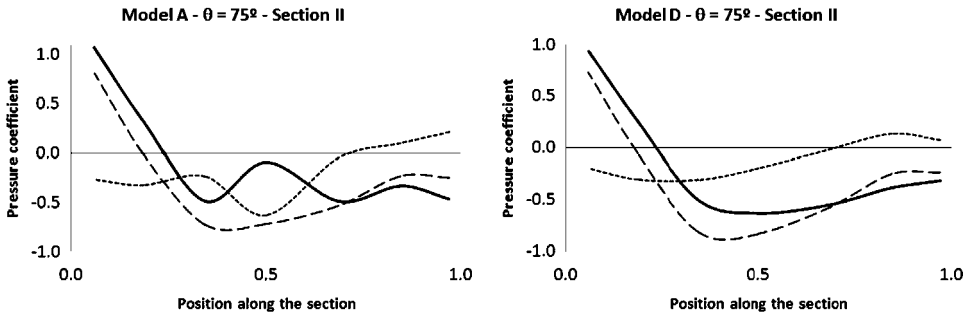

Fig. 21. Upside (dashed line), downside (dotted line) and net (solid line) pressure coefficient profiles. $\theta=75°$. Central section.

on enclosed buildings with vaulted roofs; the simultaneous occurrence of conditions (b) and (c) requires the coincidence of both distributions in that area. Fig. 24 compares the pressures on two identical roofs, one belonging to a VCR and the other to an enclosed building. It can be seen that the negative pressures, although they are not drastically different, peak at different positions and differ in value by approximately 0.2. This example, which corresponds to wind tunnel tests reported by Natalini et al. (2002), is representative of the general case. There are two main state-of-the-art sources for enclosed buildings (Blessmann, 1998; Blackmore and Tsokri, 2006) from which this pattern can be confirmed for other aspect ratios. There is no evidence to confirm condition (d), though it is likely that the VCR downside pressures behave in the same way because, there is expected to be a stagnation area under the roof for downward-side blockage and a wake flow for upwind blockage. Overall, even though no other

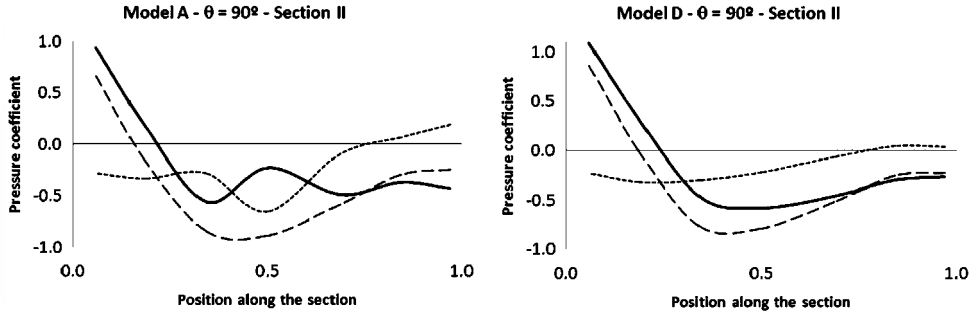

Fig. 22. Upside (dashed line), downside (dotted line) and net (solid line) pressure coefficient profiles.θ=90°. Central section.

Table 3
Comparison of worst cases of local pressure coefficients for all wind directions for a VCR of f/b =0.2 and a duo-pitch PCR with a slope of 22.5°.

	Near the edges areas		Near the ridge area	
	Max.	Min.	Max.	Min.
VCR according to Natalini (2005)	1.8	−1.8	–	−1.1
PCR according to Ginger and Letchford (1991)	1.4	−2.2	–	−2.2

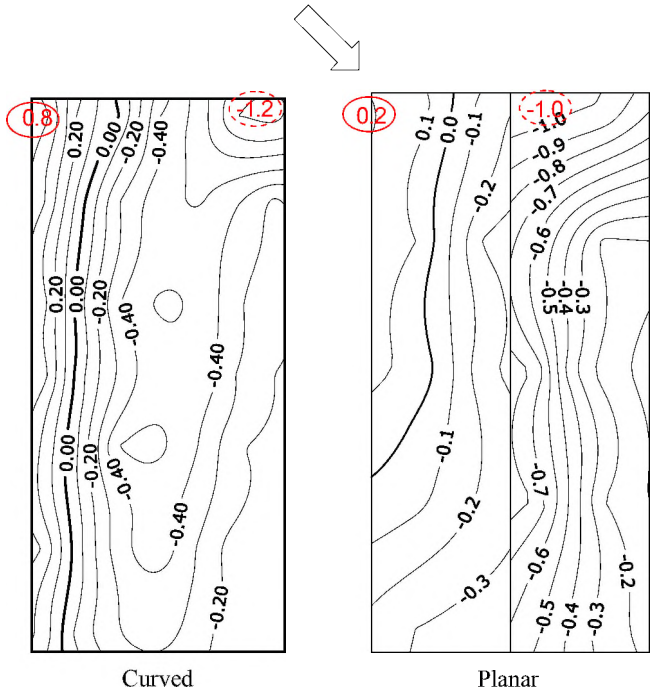

Fig. 23. Contour plots of upside mean pressure coefficients over curved and planar canopy roofs (after Marighetti et al., 2002).

Table 4
Downside pressure coefficient for fully blocked canopies (after Cook, 1990.)

Stacking arrangement	c_{pD}
Blocked on one side	
blocked on upwind side	−0.3
blocked on downwind side	+0.5
Blocked on three sides	
open on upwind side	+0.6
blocked on upwind side	−0.3
Blocked on all four sides	−0.1

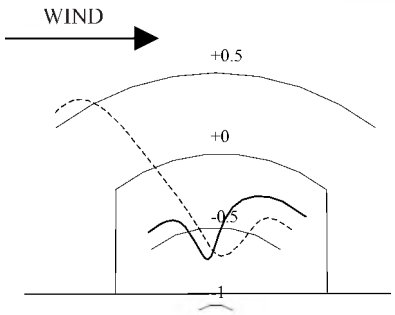

Fig. 24. Distributions across the middle section of the upside pressure coefficient on a VCR (dashed line) and the external pressure coefficient of an enclosed building with a similar roof (solid line).

soundly based recommendation is available, this rule should not be used until new supporting evidence is produced.

4.4.2. Partial blockage

The second rule concerns partially blocked canopies: 'No corrections for blockage are required for canopies blocked up to 30% from the ground. For higher degrees of blockage, the load can be linearly interpolated between the loads corresponding to full blockage (solidity ratio s=1) and no blockage (assigning this value to s=0.3).'

Balbastro and Sonzogni (2011) reported the results of mean loads on a partially blocked VCR obtained by CFD. They modelled a roof of 12 m in span, 1.5 m in rise, 5.5 m of eave height and 24 m in length (f/b=0.125, h/b=0.46 and b/a=0.5). Underneath the roof, a prismatic obstacle was placed with the dimensions of a lorry, causing a partial blockage with a total solidity ratio s=0.53. In a more recent paper (Balbastro and Sonzogni, 2012), they increased the cases of blockage under the same roof by modifying the height and length of the obstacle and its position. Unlike the cases with no blockage, these results have not been validated with experiments. Table 5 summarises the twelve cases and compares the drag and lift coefficients provided by Balbastro and Sonzogni with an estimation made by applying the aforementioned rule to the same cases.

The estimated values for cases 3, 6, 9 and 12 are the ones provided by Balbastro and Sonzogni for the unblocked case because the blockage is below 30% from the ground. In the other cases, the estimation was not straightforward because the solidity ratio was not uniform along the roof. For instance, in case 1, the

Table 5
Comparison of drag and lift coefficients, $C_D$and C_L, obtained by CFD and applying Cook's rule for partial blockage.

Case	Obstacle dimensions			Position of the obstacle	C_D		C_L	
	Length (m)	Height (m)	Width (m)		CFD	Estimated	CFD	Estimated
1	20	4.1	2.6	2 m inside from the upwind eave	0.49	−0.24	0.25	0.26
2		2.1			0.71	0.53	0.16	0.15
3		1.0			0.68	0.70	0.09	0.12
4	10	4.1			0.67	0.23	0.14	0.19
5		2.1			0.69	0.62	0.09	0.13
6		1.0			0.67	0.70	0.11	0.12
7	20	4.1		2 m inside from the downwind eave	0.65	−0.52	0.47	0.55
8		2.1			0.76	0.48	0.27	0.20
9		1.0			0.68	0.70	0.12	0.12
10	10	4.1			0.72	0.09	0.30	0.34
11		2.1			0.69	0.59	0.16	0.16
12		1.0			0.70	0.70	0.09	0.12

total solidity ratio was $s=0.53$, but the obstacle was shorter than the roof. The total solidity radio resulted from the combination of a value of $s=0.75$ at the location of the obstacle and a value of $s=0$ in the remaining part of the roof. In this particular case, the force coefficients corresponding to $s=0.75$ were estimated; the drag and lift forces were then calculated separately for the parts of the roof with $s=0.75$ and $s=0$, and the results were recombined into the values appearing in Table 5. Another problem was that the loads corresponding to full blockage were needed as inputs in the rule for partial blockage, but, as mentioned before, no one has yet reported any results on any case of fully blocked VCRs. The only possibility was to estimate the loads for $s=1$ by applying the rule for full blockage. To do so, upside pressures were adopted from Blessmann (1998).

The comparison confirms that, for blockage up to 30% from the ground, no correction is needed. The estimation of C_L is acceptable in all the cases considering that the differences are less than or equal to 0.08. However, the results diverge for C_D, especially where the obstacle is larger, regardless of whether the obstacle is on the upwind side or the downwind side. This divergence can occur either (a) because the rule for full blockage does not produce a good estimation of the loads on the fringes of the roof nearest the eaves, which have a dominant influence on C_D due to the curvature of the roof or (b) because the function between the loads corresponding to full blockage and no blockage is strongly non-linear.

It is not possible to be conclusive about a rule affected by so many assumptions (among them, that the CFD model appropriately represents the loads) based only on these particular cases, which could be flawed by a number of factors over which the authors of this paper have no control. Similar to the rule for full-blockage, this model should not be used until more research is conducted on this topic. However, the rule cannot be used in other cases due to lack of data.

5. Influence of f/b ratio

From the results presented in Fig. 10, it is possible to formulate a simple rule to estimate the overall load coefficient on a VCR with no blockage: values of 1.05 and 0.35 are the upper limits for C_D and C_L, respectively, for all the wind directions. As long as the f/b ratio is 0.2, the rule applies to any aspect ratio comprised between the cases presented in Section 4.

Balbastro and Sonzogni (2011) obtained values of 0.7 and 0.12 for C_D and C_L on a roof with f/b=0.125. This is an indication that the f/b ratio is the most relevant aspect ratio affecting the wind loads on VCRs. To establish a rule as simple as the aforementioned one for a broader range of f/b ratios, global drag and lift coefficients were produced from the local pressure coefficient produced by Balbastro (2009), who obtained results for roofs with f/b ratios of 0.181, 0.128 and 0.071. The results obtained in this way were not consistent with those from Balbastro and Sonzogni (2011) or even among themselves. It is expected that further results on this subject will soon be made available by Balbastro and Sonzogni.

6. Conclusions

In this paper, new results of mean load coefficients on VCRs are presented, and the aerodynamics of these structures were discussed, taking into account the amount of data produced in the last decade, which is not readily accessible because most of the data are published in Spanish. It has been shown that aspect ratios other than f/b have little influence on the mean loads when the roof has no blockage and that the minor differences caused by changing these aspect ratios are due to variations in the downside pressures, while the upside pressures remain unchanged. Cook's description of the general pattern of load proved to be accurate. It was confirmed that the local minimum loads near the ridge are significantly lower on VCRs than on PCRs. The maximum and minimum local loads near the edges of the roof occur at similar points on VCRs and PCRs, but the maximum is higher and the minimum is lower on the VCRs than on the PCRs. Evidence has been presented that the rule concerning flow separation misjudges the critical value of f/b for separation, which is approximately 0.1 instead of 0.25. Underneath blockage is a critical factor that modifies the values of the loads, making them much more severe. Cook's rules for estimating loads when there is a blockage, which were originally formulated for duo-pitch PCRs, should not be applied to VCRs as long as new evidence has not been produced.

Even though we significantly improved the knowledge on the wind loads on VCRs in recent years, it is not yet possible to produce recommendations of design load coefficients for codification. On the one hand, there are significant gaps concerning the values of coefficients for key situations, the foremost being underneath blockage and variations in the f/b aspect ratio. On the other hand, the discussion presented here only addressed mean load coefficients because no information on fluctuating loads has been reported so far in the literature. To estimate a peak design load from any of the known load coefficients, the equivalent-steady-gust (ESG) model (Cook, 1990) should be used. The effectiveness of the ESG model, which is a particular case of the quasi-steady approach, has been examined by Cook (1990), Letchford et al. (1993) and Hoxey et al. (1996), among others. The ESG model has a

reasonable accuracy regarding global loads, but it may misrepresent local loads in areas under the influence of building-generated turbulence.

Acknowledgements

The authors wish to acknowledge the help of Jose A. Iturri in creating the models and preparing the experimental set-up. The present work is part of an area of research supported by the Facultad de Ingeniería de la Universidad Nacional del Nordeste, CONICET and the ANPCyT, Argentina.

References

Altman, D.R., 2001. Wind uplift forces on roof canopies. M.Sc. Thesis., Clemson University, Clemson, South Carolina.

Balbastro, G.S., 2009. Coeficientes de presión en cubiertas abovedadas aisladas sometidas a la acción del viento. Tesis de Doctorado. Universidad Tecnológica Nacional. Facultad Regional Santa Fe.

Balbastro, G., Sonzogni, V., Franck, G., Storti, M., 2004. Acción del viento sobre cubiertas abovedadas aisladas: simulación numérica. Mecánica Computacional 23, 2079–2095.

Balbastro, G., Sonzogni, V., Franck, G., 2005. Simulación numérica del viento sobre una cubierta abovedada. Mecánica Computacional 24, 1261–1278.

Balbastro, G., Sonzogni, V., 2006. Coeficientes de presión en cubiertas abovedadas aisladas. Memorias de XIX Jornadas Argentinas de Ingeniería Estructural, Mar del Plata, Argentina.

Balbastro, G., Sonzogni, V., 2007. Simulación de un ensayo en túnel de viento aplicando CFD. Mecánica Computacional 26, 3779–3787.

Balbastro, G., Sonzogni, V., 2011. Efecto del viento en cubiertas curvas aisladas con obstrucciones. Mecánica Computacional 30, 2599–2607.

Balbastro, G., Sonzogni, V., 2012. Cargas de viento en cubiertas curvas aisladas con obstrucciones. Memorias XXXV Jornadas Sul Americanas de Engenharia Estrutural, Rio de Janeiro, Brazil.

Blackmore, P.A., Tsokri, E., 2006. Wind loads on curved roofs. Journal of Wind Engineering and Industrial Aerodynamics 94 (11), 833–844.

Blessmann, J., 1998. Wind load on isolated and adjacent industrial pavilion curved roof. In: Riera, J.D., Davenport, A.G. (Eds.), Wind Effects on Buildings and Structures. Balkema, Rotterdam, pp. 137–171.

CIRSOC 102, 1983. Acción del viento sobre las construcciones. Instituto Nacional de Tecnología Industrial, Buenos Aires.

CIRSOC 102, 2005. Reglamento Argentino de acción del viento sobre las construcciones. Instituto Nacional de Tecnología Industrial, Buenos Aires.

Cook, N.J., 1977/1978. Determination of the model scale factor in wind-tunnel simulations of the adiabatic atmospheric boundary layer. Journal of Wind Engineering and Industrial Aerodynamics 2, 311–321.

Cook, N.J., 1990. The designer's guide to wind loading of building structures, part 2: static structures. Building Research Establishment, London.

Counihan, J., 1975. Adiabatic atmospheric boundary layers: a review and analysis of data from the period 1880–1972. Atmospheric Environment 9, 871–905.

De Bortoli, M.E., Natalini, B., Paluch, M.J., Natalini, M.B., 2002. Part-depth wind tunnel simulations of the atmospheric boundary layer. Journal of Wind Engineering and Industrial Aerodynamics 90, 281–291.

Ginger, J.D., Letchford, C.W., 1991. Wind loads on canopy roofs. Department of Engineering Science, University of Qld., Research report no. CE132.

Gumley, S.J., Wood, C.J., 1980. Mean and extreme pressure study on model Dutch barns. Uni. of Oxford Dept. of Eng. Sc., OUEL report no. 1333/80.

Gumley, S.J., 1981. Panel loading mean pressure study for canopy roofs. Uni. of Oxford Dept. of Eng. Sc., OUEL report no. 1380/81.

Gumley, S.J., 1982. Design extreme pressures—a parametric study for canopy roofs. Uni. of Oxford Dept. of Eng. Sc., OUEL report no. 1394/82, 1982.

Gumley, S.J., 1984. A parametric study of extreme pressures for the static design of canopy structures. Journal of Wind Engineering and Industrial Aerodynamics 16, 43–56.

Helliwell, N.C., 1971. Wind over London. Proceedings of the Third International Conference on Wind Effects on Buildings and Structures, Tokyo, Japan.

Hoxey, R.P., Richards, P.J., Richardson, G.M., Robertson, A.P., Short, J.L., 1996. The folly of using extreme-value methods in full-scale experiments. Journal of Wind Engineering and Industrial Aerodynamics 60, 109–122.

Irminger, J.O.V., Nokkentved, C., 1936. Wind Pressure on Buildings. Experimental Researches (Second Series). Danmarks Naturvidenskabelige Samfund, Coppenhagen.

Irwin, H.P.A.H., 1981. The design of spires for wind simulation. Journal of Wind Engineering and Industrial Aerodynamics 7, 361–366.

Letchford, C.W., Iverson, R.E., McDonald, J.R., 1993. The application of the quasi-steady theory to full scale measurements on the Texas Tech Building. Journal of Wind Engineering and Industrial Aerodynamics 48, 111–132.

Marighetti, J.O., Canavesio, O., Natalini, B., Natalini, M.B, 2002. Comparación entre coeficientes de presión media en cubiertas aisladas planas y curvas. Memorias de las XVII Jornadas Argentina de Ingeniería Estructural, Rosario, Argentina.

Natalini, M.B., 2005. Acción del viento sobre cubiertas curvas aisladas. Tesis de Doctorado. Universidad Nacional del Nordeste, Argentina.

Natalini, M.B., Canavesio, O., Natalini, B., Paluch, M.J., 2001. Wind tunnel modelling of mean pressures on curved canopy roofs. Proceeding of the Americas Conference on Wind Engineering, Clemson, USA.

Natalini, M.B., Canavesio, O., Natalini, B., Paluch, M.J., 2002. Pressure distribution on curved canopy roof. Proceedings of The Second International Symposium on Advances in Wind and Structures. Pusan, Korea.

Natalini, M.B., Morel, C., Natalini, B., 2005. Mean wind loads on vaulted canopy roofs under different wind directions. Revista Sul-Americana de Engenharia Estrutural 2, 29–40.

NV 65, 1970. Règles définisant les effets de la neige et du vent sur les constructions et annexes. Societé de Diffusion des Techniques du Bâtiment et des Travaux Publics, France.

Robertson, A.P., Hoxey, R.P., Moran, P., 1985. A full scale study of wind loads on agricultural ridged canopy roof structures and proposal for design. Journal of Wind Engineering and Industrial Aerodynamics 21, 167–205.

Teunissen, H.W., 1977. Measurements of planetary boundary layer wind and turbulence characteristics over a small suburban airport. (MSRB) Atmospheric Environment Service, Internal Report No. MSRB - 77 - 4, Downsview, Ontario.

Uematsu, Y., Izumi, E., Stathopoulos, T., 2007. Wind force coefficients for designing free-standing canopy roofs. Journal of Wind Engineering and Industrial Aerodynamics 95, 1486–1510.

Wittwer, A.R., Möller, S.V., 2000. Characteristics of the low-speed wind tunnel of the UNNE. Journal of Wind Engineering and Industrial Aerodynamics 84, 307–320.